Biochemical Pharmacology 78 (2009) 162–170

Contents lists available at ScienceDirect

Biochemical Pharmacology

journal homepage: www.elsevier.com/locate/biochempharm

Molecular pharmacology and antitumor activity of *Zalypsis*® in several human cancer cell lines

Juan F.M. Leal [a], Verónica García-Hernández [b], Victoria Moneo [a], Alberto Domingo [b], Juan Antonio Bueren-Calabuig [c], Ana Negri [c], Federico Gago [c], María José Guillén-Navarro [a], Pablo Avilés [a], Carmen Cuevas [a], Luis Francisco García-Fernández [a], Carlos María Galmarini [a,*]

[a] *Cell Biology Department, Pharmamar SA, Avda. de los Reyes, 1, 28770 Colmenar Viejo, Madrid, Spain*
[b] *Department of Biochemistry and Molecular Biology, University of Alcalá, Spain*
[c] *Department of Pharmacology, University of Alcalá, Spain*

ARTICLE INFO

Article history:
Received 13 February 2009
Accepted 6 April 2009

Keywords:
Antineoplastic agents
Tetrahydroisoquinolines
DNA breaks
Apoptosis

ABSTRACT

Zalypsis® is a new synthetic alkaloid tetrahydroisoquinoline antibiotic that has a reactive carbinolamine group. This functionality can lead to the formation of a covalent bond with the amino group of selected guanines in the DNA double helix, both in the absence and in the presence of methylated cytosines. The resulting complex is additionally stabilized by the establishment of one or more hydrogen bonds with adjacent nucleotides in the opposite strand as well as by van der Waals interactions within the minor groove. Fluorescence-based thermal denaturation experiments demonstrated that the most favorable DNA triplets for covalent adduct formation are AGG, GGC, AGC, CGG and TGG, and these preferences could be rationalized on the basis of molecular modeling results. Zalypsis®–DNA adducts eventually give rise to double-strand breaks, triggering S-phase accumulation and apoptotic cell death. The potent cytotoxic activity of Zalypsis® was ascertained in a 24 cell line panel. The mean IC_{50} value was 7 nM and leukemia and stomach tumor cell lines were amongst the most sensitive. Zalypsis® administration in four murine xenograft models of human cancer demonstrates significant tumor growth inhibition that is highest in the Hs746t gastric cancer cell line with no weight loss of treated animals. Taken together, these results indicate that the potent antitumor activity of Zalypsis® supports its current development in the clinic as an anticancer agent.

1. Introduction

Zalypsis® (Fig. 1A) is a new synthetic dimeric isoquinoline alkaloid that is currently in Phase I clinical development for the treatment of solid tumors and hematological malignancies. This compound is structurally related to jorumycin, a natural compound isolated from the skin and mucus of the Pacific nudibranch *Jorunna funebris* [1], and also to renieramycins isolated from sponges and tunicates [2,3], safracins and saframycins isolated from bacteria and marine sponges [4], and ecteinascidins isolated from marine tunicates [5]. These carbinolamine-containing compounds react, through an iminium intermediate that is generated by dehydration [4,6–8], with the exocyclic amino group of selected guanines in the minor groove of DNA. The resulting adduct is additionally stabilized through the establishment of van der Waals interactions and one or more hydrogen bonds with neighboring nucleotides in the opposite strand of the DNA double helix [8,9], thus creating the equivalent to a functional interstrand crosslink [10] that can lead to strong inhibition of the early phases of transcription [11,12].

In this study we characterized both molecular interactions with the DNA and the cytotoxic activity of Zalypsis® in an attempt to shed light into its mechanism of antitumor action. The DNA-binding characteristics were studied using a combination of electrophoretic mobility shift assays in polyacrylamide gels and a fluorescence-based method that employs tailor-made oligonucleotides. We also looked at the type of DNA damage subsequently generated in living cells as a consequence of Zalypsis®–DNA adduct formation and whether cell cycle arrest and cell death induced by this compound mechanistically depend on caspase activation. Then, *in vitro* cytotoxic activity was evaluated in a panel of 24 different cancer cell lines. Finally, the *in vivo* antitumor activity of Zalypsis® was investigated using several murine xenograft models of human prostate, stomach, bladder and pancreas carcinomas.

* Corresponding author. Tel.: +34 91 846 6158; fax: +34 91 846 6001.
E-mail address: cgalmarini@pharmamar.com (C.M. Galmarini).

0006-2952/$ – see front matter © 2009 Elsevier Inc. All rights reserved.
doi:10.1016/j.bcp.2009.04.003

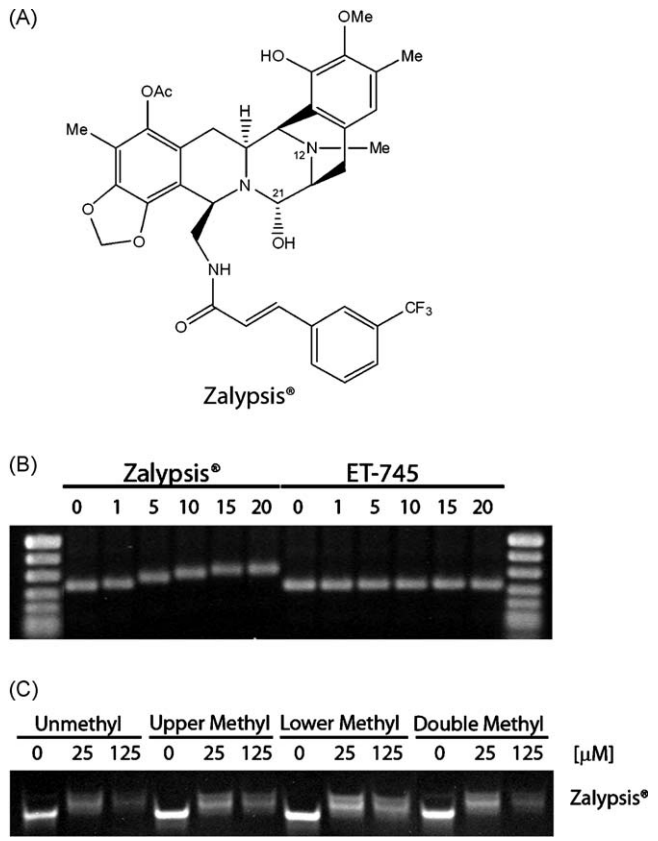

Fig. 1. Cytotoxic effect and DNA-binding properties of Zalypsis®. (A) Structure of Zalypsis® showing the positions of *C21* and *N12* atoms discussed on the main text. (B) Binding to naked DNA. Drugs were incubated with a naked 250 bp PCR product at 25 °C during 1 h and the electrophoresis run in 2% agarose-TAE. (C) Binding to methylated DNA. The methylated ds-oligo with a unique binding site for Zalypsis® was incubated with the drug at 25 °C during 1 h, then electrophoresis was run in a 20% acrylamide-TAE gel.

2. Materials and methods

2.1. Drugs

Zalypsis® is a Pharmamar SAU proprietary drug synthesized at our facilities. ET-745 is a synthetic isoquinoline derived from trabectedin (ET-743) that lacks the carbinolamine group (Supplementary Material, Figure 1) and does not alkylate DNA [13]. Z-Vad-fmk is a pan-caspase inhibitor purchased from Sigma (St. Louis, MO, USA).

2.2. DNA electrophoretic mobility shift assay

The binding assays were performed either with a 250 bp PCR product from the human adiponectin gene or with a double-stranded oligonucleotide (ds-oligo) synthesized by Sigma (St. Louis, MO, USA). Briefly, appropriate concentrations of the compound were added at 25 °C during 1 h to 250 bp DNA or ds-oligo. Then, DNA was subjected to electrophoresis in a 2% (w/v) agarose/TAE gel, stained with 1 μg/ml ethidium bromide and photographed. The sequences of the oligonucleotides used in the assay are the following: NonMeth-Fw 5′-TAAATATTTCCGGATATAATTAT-3′; NonMeth-Rev 5′-ATAATTATATCCGGAAATATTTA-3′; Meth-Fw 5′-TAAATATTTC**MeC**GGATATAATTAT-3′; Meth-Rev 5′-ATAATTATATC**MeC**GGAAATATTTA-3′.

2.3. DNA melting assay

Synthetic oligodeoxynucleotides with one strand 5′-end-labeled with the fluorophore 6-carboxyfluorescein (6-FAM, F) and the complementary strand 3′-end-labeled with the quencher tetramethylrhodamine (TAMRA, Q) were synthesized at Bonsai Technologies (Madrid, Spain) (Supplementary Table 1). For the experiments, we followed the methodology previously described in a 7500 Fast Real-Time PCR System (ABI Prism, Applied Biosystems, Foster City, CA, USA) [10,14]. The raw data obtained were analyzed to estimate the increases in melting temperatures (ΔT_m) brought about by drug binding as well as the ligand concentration that produces half the maximal change in melting temperature (C_{50}). The inverse of this value ($1/C_{50}$) was taken as a measure of the relative DNA-binding affinity. We additionally used the parameter $\Delta T_m(\max)$ to reflect the relative stability of the DNA-ligand complexes [14]. The complete analysis was carried out using an in-house developed Visual Basic Application running on Microsoft Excel (Microsoft, Redmond, WA, USA).

2.4. Computational methods

We studied in atomic detail the feasibility of achieving the geometries required to activate dehydration of the carbinolamine prior to the nucleophilic attack that leads to covalent bond formation. To this end, the initial structures of the precovalent complexes between Zalypsis® and a series of oligonucleotides of general sequence 5′-d(ATAATAXYZATAATA)/5′-d(TATTATZ′Y′X′TATTAT), where XYZ/Z′Y′X′ stands for AGA/TCT, AGG/CCT and AGC/GCT, were built as previously reported for trabectedin [15]. The complexes were then refined using energy minimization techniques in the AMBER force field and their stability was studied by means of 5 ns of unrestrained molecular dynamics simulations in an explicit water box using the same conditions as described previously.

2.5. Cell culture and cytotoxicity

All the tumor cell lines used in this study were obtained from the American Type Culture Collection (ATCC, Rockville, MD, USA). For the cytotoxicity experiments, cells were seeded in 96-well trays. Serial dilutions of the compound dissolved in dimethyl sulfoxide (DMSO) were prepared and added to the cells in fresh medium, in triplicates. Exposure to the compounds was maintained during 72 h. Then 3-(4,5-dimethylthiazol-2-yl)-2,5-diphenyltetrazolium bromide (MTT) (Sigma, St. Louis, MO, USA) was added to the cells and formazan crystals dissolved in DMSO. Absorbance at 540 nM was measured with a POLARStar Omega Reader (BMG Labtech, Offenburg, Germany). Determination of IC_{50} values was performed by iterative non-linear curve fitting with the Prism 5.0 statistical software (GraphPad, La Jolla, CA, USA). The data presented are the average of three independent experiments performed in triplicate.

2.6. Fluorescent microscopy

Cells were treated with the appropriate concentration of Zalypsis® during 6 h, washed out and cultured for 18 additional hours. Cells were then fixed (4% paraformaldehyde), permeabilized (0.5% Triton X-100) and incubated with the primary anti-γ-H2AX monoclonal antibody (Upstate, Temecula, CA) for 1 h at 37 °C. Then cells were washed and incubated with the secondary anti-mouse AlexaFluor 594 (Invitrogen, Carlsbad, CA, USA) for 30 min at 37 °C. Finally the slides were incubated with Hoesch 33342 (Sigma, St. Louis, MO, USA) and mounted with Mowiol mounting medium. Pictures were taken with a Leica DM IRM fluorescence microscope equipped with a 100× oil immersion objective and a DFC 340 FX digital camera (Leica, Wetzlar, Germany).

2.7. Comet assay

For the determination of double-strand breaks (DSBs) a single cell gel electrophoresis assay was used (Trevigen's CometAssay™), following the manufacturer's instructions after treatment of cells for 12 h with the appropriate concentration of Zalypsis®. Pictures were taken with a Leica DM IRM fluorescence microscope equipped with a DFC 340 FX digital camera (Leica, Wetzlar, Germany). Quantitation of the DNA in the tails of the comets was performed with Adobe Photoshop CS3 (Adobe Systems Incorporated, San Jose, CA, USA). For each condition 30 cells were analyzed, and the experiments were repeated several times.

2.8. Cell cycle analysis

For the cell cycle experiments, cells were treated with the appropriate amount of the compound for 24 h, and then stained with 0.4 μg/ml propidium iodide. Samples were analyzed with a FACScalibur flow cytometer (Beckton and Dickinson, Franklin Lakes, NJ, USA) and the FlowJo7 cytometry analysis software.

2.9. Apoptosis

For the chromatin condensation assay, cells were treated with the appropriate amount of the compound for 24 h and stained with DAPI. Early apoptotic cells show chromatin condensation that was assessed with a DM IRM microscope (Leica, Wetzlar, Germany). For the M30-Apoptosense solid-phase sandwich enzyme immunoassay (Peviva, Bromma, Sweden), the kit's instructions were followed. Briefly, cells were exposed to the appropriate concentration of the compound for 24 h. Cells lysates were obtained and transferred to an assay well, M30 HRP conjugate added and incubated for 4 h. Once the antigen-M30 was bound to the M5-coated surface of the wells, they were extensively washed and incubated with TMB substrate in the dark for 20 min. Finally, the reaction was stopped with the addition of a stop solution and plates were read at 450 nM within 30 min with a Victor3 platform (PerkinElmer).

2.10. Western blot assays

For immunoblotting, cells were treated with the appropriate concentration of the compound for 24 h and lysed with RIPA lysis buffer. Protein content was determined by the modified Bradford method. Samples were separated in 7.5% SDS-PAGE, transferred onto an Immobilon-P membrane. Then, membranes were incubated with the appropriate primary antibody 1 h, washed and incubated with the secondary antibody. Finally protein was visualized using the ECL System (GE Healthcare, Fairfield, CT, USA). We used anti-PARP rabbit polyclonal, anti-p53FL rabbit polyclonal and anti-p21/WAF1 rabbit polyclonal antibodies from Santa Cruz (Santa Cruz, CA, USA), and an anti-α-tubulin monoclonal antibody from Sigma (St. Louis, MO, USA). Secondary antibodies were HRP-conjugated goat anti-rabbit secondary antibody (R&D Minneapolis, MN, USA) and HRP-conjugated goat anti-mouse secondary antibody (Santa Cruz, CA, USA).

2.11. Antitumor activity in xenograft murine models

Four- to six-week-old athymic *nu*/*nu* mice (Harlan Sprague Dawley, Madison, WI, USA) were s.c. xenografted into their right flank with ca. $(0.5–1) \times 10^7$ cells in 0.2 ml of a mixture (50:50; v:v) of Matrigel basement membrane matrix (Beckton Dickinson, Frankin Lakes, NJ, USA) and serum-free medium. When tumors reached ca. 150 mm^3, mice were randomly assigned into treatment or control groups. Zalypsis® was intravenously administered either in 3 consecutive weekly doses (0.9 mg/kg/day) or in 2 cycles of 5 consecutive daily doses (0.3 mg/kg/day) in pancreas or in breast and prostate xenograft studies, respectively. Control animals received an equal volume of vehicle. Caliper measurements of the tumor diameters were done twice weekly and tumor volumes calculated according to the following formula: $(ab)^2/2$, where a and b were the longest and shortest diameters, respectively. Animals were humanely euthanized, according to Institutional Animal Care and Use Committee of PharmaMar, Inc. (Cambridge, MA, USA) guidelines, when their tumors reached 3,000 mm^3 or if significant toxicity (e.g. severe body weight reduction) was observed. Differences in tumor volumes between treated and control groups were evaluated using the unpaired t-test. Statistical significance was defined as $p < 0.05$. Statistical analyses were performed by LabCat® v8.0 SP1 (Innovative Programming Associates, Inc. NJ, USA). All animal studies were conducted under approval from an IACUC in an AAALAC accredited animal facility.

3. Results

3.1. Zalypsis® binds covalently to DNA

The mechanism of action of Zalypsis® is expected to rely on the alkylation of selected guanines in the DNA double helix. Thus, we investigated its binding to DNA by means of band shift assays that allow the qualitative assessment of the molecular weight increase of Zalypsis®–DNA adducts. Fig. 1B shows a typical band shift experiment using increasing amounts of Zalypsis® in order to saturate the 250 bp DNA probe with the compound. ET-745, which lacks the crucial hydroxyl group required for activation and covalent DNA modification, was used as a negative control (Supplementary Figure 1). As expected, Zalypsis® bound to naked DNA and delayed its electrophoretic migration in the gel. Although 1 μM of Zalypsis® was enough to produce a slight delay in band migration, DNA saturation required ~15 μM of the compound.

We further assessed whether Zalypsis® could alkylate methylated DNA, using a ds-oligo containing a methylated cytosine in the sequence *me*CGG. Fig. 1C shows the result of a typical experiment. Zalypsis® bound to methylated and unmethylated CGG sequences with similar efficiencies, suggesting that methylation of the cytosine in a CpG sequence context in the major groove does not interfere with guanine modification in the DNA minor groove.

3.2. Zalypsis® binds to guanines in selected DNA triplets

To investigate the ability of Zalypsis® to stabilize the double helix, we designed several fluorophore-labeled oligonucleotides encompassing most of the possible DNA triplet combinations involving a central guanine (Supplementary Table 1). Fig. 2A summarizes the results of the DNA melting experiments. The average $1/C_{50}$ and $\Delta T_m(\max)$ values for Zalypsis® were ~0.6 μM^{-1} and ~10 °C, respectively. There were differences in the affinity of Zalypsis® for the different triplets assayed, with the highest affinity being observed for GGC, AGC, AGG and TGG triplets, and the lowest, almost negligible, being displayed by the CGA triplet. Nonetheless, some of the selected triplets (e.g. AGC or AGG) do not provide a good binding site if embedded in an alternative sequence context (e.g. AGCA vs. AGCG and AGGA vs. AGGG). On the other hand, the highest stabilities were observed for adducts formed with the oligos containing the triplets AGA, TGT, AGG, GGC and TGG. Thus, according the affinity indicator $1/C_{50}$, the most favorable triplets for Zalypsis® bonding to DNA appear to be AGG, GGC, AGC, CGG and TGG whereas the thermal stability of the DNA-adduct involving an AGA or TGT site is slightly above average

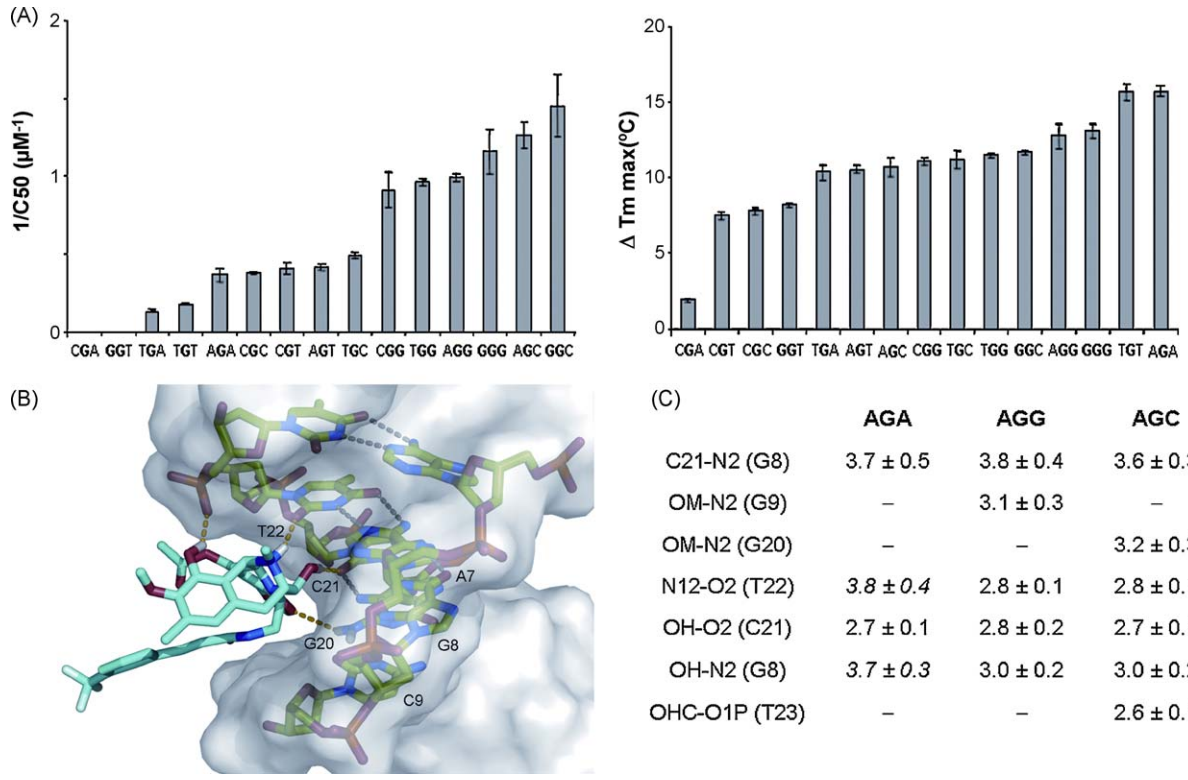

	AGA	AGG	AGC
C21-N2 (G8)	3.7 ± 0.5	3.8 ± 0.4	3.6 ± 0.3
OM-N2 (G9)	–	3.1 ± 0.3	–
OM-N2 (G20)	–	–	3.2 ± 0.3
N12-O2 (T22)	*3.8 ± 0.4*	2.8 ± 0.1	2.8 ± 0.1
OH-O2 (C21)	2.7 ± 0.1	2.8 ± 0.2	2.7 ± 0.1
OH-N2 (G8)	*3.7 ± 0.3*	3.0 ± 0.2	3.0 ± 0.2
OHC-O1P (T23)	–	–	2.6 ± 0.1

Fig. 2. Characteristics and modeling of DNA–Zalypsis® complexes. (A) Relative binding affinities for different DNA triplet sequences. Zalypsis® was incubated with the labeled ds-oligos at 25 °C during 1 h, then the melting assay was started in a 7500 Fast Real-Time PCR System by increasing the temperature up to 95 °C in small steps of 1 °C min^{-1}. Analysis of the $1/C_{50}$ parameter was done with an in-house developed Visual Basic Application (VBA) running on Microsoft Excel. An additional parameter, ΔT_m(max), which is related to the stability of the drug-DNA complex, was also analyzed using the VBA. The values correspond to the mean and standard deviation from at least two independent experiments for each sequence. (B) View of the central part of the precovalent Zalypsis®:AGC model complex in which a semitransparent solvent-accessible surface envelops the DNA atoms. Drug and DNA carbon atoms have been colored cyan and green, respectively. Only hydrogens attached to *N12* and *O21* of Zalypsis® and the amino groups of G8 and G20 are shown. Crucial hydrogen bonds are displayed as dotted yellow lines for the drug-DNA complex and dashed black lines for the DNA base pairs. (C) Attacking distances and relevant intermolecular distances (Å) between hydrogen-bonding donor and acceptor atoms in the three precovalent complexes studied (the italics for the AGA complex highlight longer distances than those needed to establish a hydrogen bond).

and those involving CGC, CGT, GGT and CGA sites are well below average.

3.3. Molecular modeling data

The molecular models of the equilibrated Zalypsis®–DNA precovalent complexes in aqueous solution provided a rationale for the distinct binding of the drug to three representative central triplets that provide good (AGC), intermediate (AGG) or poor (AGA) binding sites for this drug, the only difference among them being the nature of the base pair on the 3′-side of the guanine that will undergo alkylation. As shown in Table 1, the geometry required for nucleophilic attack of the exocyclic amino group of the central guanine (G8) at the carbinolamine of the drug (*C21*) was rapidly attained in all cases, as assessed by an interatomic distance of less than 4 Å between the two reactive atoms. Likewise, the carbinol OH was seen to act as a hydrogen bond acceptor from N2(G8) and as a hydrogen bond donor to O2 in C21, that is, the cytosine pairing with G8 (Fig. 2B). These findings are consistent with the fact that Zalypsis® is able to react with these triplet sites, and the geometry that we find in these precovalent complexes lends strong support to the proposal that the latter hydrogen bond weakens the *N12–H12* covalent bond, thus facilitating transfer of the *H12* proton to the carbinol OH, whereas the first hydrogen bond debilitates the *C21–OH* bond, thus favoring the exit of the water molecule. On the other hand, the protonated *N12* of Zalypsis® remained hydrogen-bonded to the O2 acceptor atom of T22 in the AGG and AGC triplets but not in the AGA triplet (Fig. 2C). This finding, together with the fact that AGA cannot provide a hydrogen-bonding partner to the methylenedioxy oxygen facing the minor groove may account for the fact that AGA is a poorer binding site even though the DNA in the resulting complex is stabilized to a greater extent than those containing the other sequence contexts studied (Fig. 2A). When this hydrogen-bonding partner is found, as is the case for the AGC and AGG sequences which possess the amino group of either G20

Table 1
Cell cycle perturbations[a] induced by Zalypsis®.

	Cell cycle phase	Control	15 nM	150 nM
A549	Sub-G_1	1.7	13	5.7
	G_0/G_1	60	24	49
	S-phase	25	49	30
	G_2/M	8.6	7.6	7.1
HT29	Sub-G_1	0.3	15	21
	G_0/G_1	64	17	38
	S-phase	38	63	36
	G_2/M	2	9.2	3.8
MDA-MB-231	Sub-G_1	2.3	2.2	7
	G_0/G_1	37	12	23.3
	S-phase	30	47	33
	G_2/M	13	22	18
IGROV-1	Sub-G_1	2.8	56	68
	G_0/G_1	39	11	6.5
	S-phase	33	21	18
	G_2/M	16	8.5	1.7

[a] Cells were treated with the appropriate amount of the compound for 24 h, and then stained with 0.4 μg/ml propidium iodide. Samples were analyzed with a FACScalibur flow cytometer (Beckton and Dickinson, Frankin Lakes, NJ, USA) and the FlowJo7 cytometry analysis software. Values represent % of cells in each phase of the cell cycle.

or G9, respectively, the additional hydrogen bond formed (Fig. 2B and C) facilitates the full insertion of the drug into the minor groove and leads to enhanced reactivity. As regards the small stabilization brought about by Zalypsis® on the CGA-containing oligonucleotide, this can be rationalized by proposing that it arises only from the precovalent complex, which cannot evolve into a covalent adduct because of an incorrect geometry for attack (14).

3.4. The initial Zalypsis®–DNA adducts eventually give rise to double-strand breaks in living cells

We analyzed the formation of γ-H2AX foci as a surrogate indicator of DSB formation [16,17]. Fig. 3A shows typical results of MCF7 and A549 cells treated with Zalypsis® for 6 h at the indicated concentrations. At 5 nM, only a few MCF7 or A549 cells showed γ-H2AX staining and, in the positive cells, few foci were visible (data not shown). In contrast, at 25 nM, most of the cells were stained for γ-H2AX and each of the positive cells carried a large number of foci, indicating that several DSBs per cell were induced at this drug concentration (Fig. 3A). At 100 nM, nearly every single cell stained positive for γ-H2AX, with a large number of foci per nucleus, again an indication of extensive DNA damage and induction of numerous DSBs (data not shown).

Zalypsis®-dependent formation of DSBs was additionally evaluated using the comet assay, which provides a direct measurement of damaged DNA. Both A549 and MCF7 cell lines were treated with Zalypsis® at 10 and 100 nM for 24 h and the percentage of the total DNA that was in the tail of the comets was measured. A typical comet assay result (Fig. 3B) shows a clear concentration-dependent increase in DSBs in both cell lines following treatment with Zalypsis®. The use of Mann–Whitney *U*-test demonstrated that differences between each treated-measure against the baseline were statistically significant.

3.5. Zalypsis®-treated cells accumulate in S-phase

Table 1 summarizes the results of the assessment of possible cell cycle perturbations after 24 h of exposure to Zalypsis®. At both low (15 nM) and high (150 nM) drug concentrations there was a clear increase of the S-phase population in A549 (lung), HT29 (colon) and MDA-MB-231 (breast) cancer cells. Of note, the S-phase accumulation was higher at 15 nM, probably due to a higher cell survival. In IGROV-1 cells we did not observe any S-phase accumulation, most likely due to the extensive cell death induced by the compound at both concentrations after 24 h treatment (data not shown).

3.6. Zalypsis® induces apoptosis in tumor cells

Since the antitumor mechanism of action of DNA-damaging agents is known to involve induction of apoptosis [18], we investigated whether Zalypsis® treatment was able to induce a canonical apoptosis response in tumor cells. Firstly, we determined whether the drug was able to generate late apoptosis by detecting

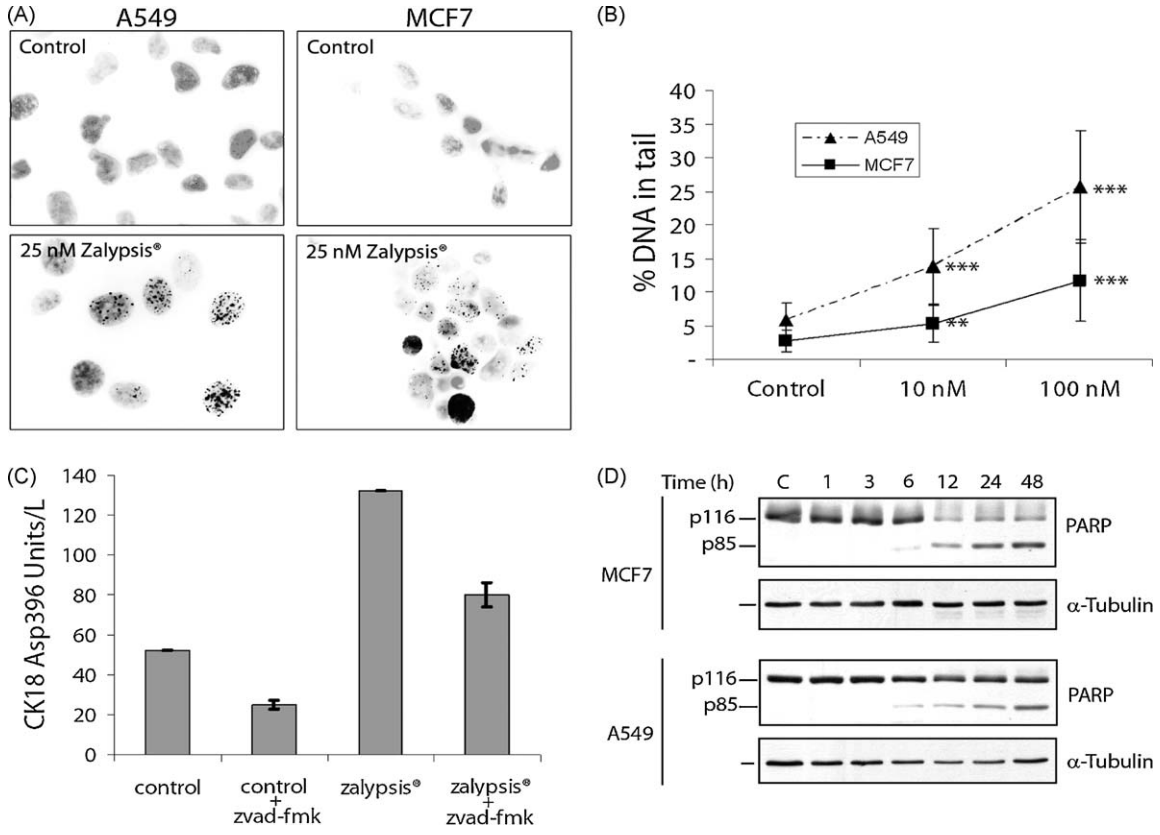

Fig. 3. Zalypsis® treatment induces DNA double-strand breaks and apoptosis in living cells. (A) A549 or MCF7 cells were treated with the drug at the indicated concentrations during 6 h, followed by additional 18 h of incubation without the drug. After fixation, cells were immunostained for γ-H2AX and nuclei were visualized with Hoestch 33342. (B) Zalypsis®-treated cells were simultaneously analyzed through comet assay to determine the amount of DSBs induced by the drug. After 12 h of treatment with the indicated concentrations of Zalypsis®, cells were washed with PBS, detached mechanically and included in low melting point agarose. After a treatment of lysis, cells were subjected to electrophoresis and the comets were stained with SYBR green. Quantitation of the amount of DNA in the comets was performed with Photoshop CS3. $^{**}p < 0.001$; $^{***}p < 0.0001$. (C) Apoptosis induced by Zalypsis® is caspase-dependent. A549 cells were treated with the drugs during 24 h, washed and processed following the protocol of the M30-Apoptosense solid-phase sandwich enzyme immunoassay. (D) Caspase activation and PARP-1 processing. MCF7 and A549 cells were treated with Zalypsis® 100 nM during 24 h and then washed and lysed with RIPA buffer supplemented with a protease inhibitor cocktail. Western blot was then performed using a primary anti-PARP-1 polyclonal antibody.

the flow-cytometric sub-G_1 cell population (Table 1). A549 and HT-29 cell treatment resulted in an increase in the sub-G_1 population. On the other hand, MDA-MB-231 cells died with a slower kinetics while IGROV-1 cells died faster (Table 1). These data indicate that the percentage of cells entering the sub-G_1 peak after 24 h of treatment with Zalypsis® was cell type- and concentration-dependent. After treatment of MCF7 and A549 cells with 100 nM Zalypsis® for 24 h, an apoptotic nuclear morphology with strong chromatin condensation was clearly visible in fluorescent microscopy in both cell types (data not shown).

We further analyzed the onset of apoptosis using a commercially available solid-phase sandwich enzyme immunoassay that detects the caspase cleavage of cytokeratin-18 as a sensitive and specific marker of early canonical apoptosis [19]. Treatment with 100 nM Zalypsis® induced a marked increase of the apoptosis-related CK-18 Asp396 epitope in A549 cells. Moreover, simultaneous treatment with the pan-caspase inhibitor Z-VAD-fmk strongly reversed this effect (Fig. 3C), which clearly indicates that the pro-apoptotic effect of Zalypsis® was dependent on caspase activity.

Finally, we studied the caspase-dependent cleavage of the nuclear protein PARP as a marker of canonical apoptosis. The p85 band, generated through proteolytic cleavage of p116 PARP by activated caspases, was clearly visible as early as 6 h after the treatment of MCF7 and A549 cells with 100 nM Zalypsis® (Fig. 3D). After 48 h of treatment a considerable proportion of the PARP protein had already been cleaved by caspases, indicating that most of the cells were undergoing canonical apoptosis.

3.7. Zalypsis® shows a potent cytotoxic activity

The *in vitro* cytotoxicity of Zalypsis® was determined using a panel of 24 tumor cell lines that represent 11 relevant types of human cancer (Table 2). Most of the cell lines were very sensitive to Zalypsis® treatment, with IC_{50} values in the low nanomolar range. The panel average IC_{50} was ~7 nM, with MOLT-4 (acute lymphoblastic leukemia) cells showing the lowest IC_{50} and CAKI-1 (renal carcinoma) and HCT116 (colon carcinoma) cells presenting the highest IC_{50}s in the mid-nanomolar range.

Table 2
Cytotoxicity of Zalypsis® in a panel of 24 human cancer cell lines[a].

	Cell line	IC_{50} (nM)	Tissue average (nM)
Prostate	PC3	2.4 ± 1.1	2.1 ± 0.4
	22RV1	1.7 ± 0.8	
Pancreas	PANC-1	4.1 ± 0.8	2.7 ± 1.9
	MiaPaCa-2	1.3 ± 0.4	
Ovary	IGROV-1	3.5 ± 0.1	2.8 ± 0.9
	A2780	2.1 ± 1.3	
Lung	NCI-H460	3 ± 1.2	2.5 ± 0.4
	NCI-H23	2.2 ± 0.3	
	A549	2.4 ± 0.8	
Liver	SK-HEP-1	2.5 ± 0.8	2.5 ± 0.1
	HEPG2	2.6 ± 1.5	
Leukemia	MOLT4	0.5 ± 0.2	1 ± 0.7
	K562	1.6 ± 1.5	
Kidney	RXF393	2.1 ± 0.5	21.9 ± 27
	CAKI-1	41 ± 5	
Stomach	HS746T	1.5 ± 0.1	1.6 ± 0.07
	HGC-27	1.6 ± 0.5	
Colon	LoVo	2.4 ± 0.8	23 ± 34
	HT29	3.8 ± 0.2	
	HCT-116	62 ± 30	
Bladder	SW780	10 ± 0	10
Breast	MDA-MB-231	4.8 ± 0.8	4.1 ± 0.9
	MCF-7	4.5 ± 0.1	
	BT-474	3 ± 1.2	

[a] Values represent mean ± SD of three different experiments.

3.8. Zalypsis® exhibits in vivo antitumor activity in xenograft murine models

We performed xenograft studies to test whether the cytotoxicity of Zalypsis® translates into *in vivo* antitumor activity. 22RV1 (prostate), SW780 (bladder), Hs746t (gastric), and MiaPaCa-2 (pancreas) cells were xenografted into the right flank of athymic nu/nu mice. Once the tumors reached ca. 150 mm^3, the mice were randomized into groups of 10 and Zalypsis® was intravenously administered either in 3 consecutive weekly doses (0.9 mg/kg/day) (prostate and bladder) or in 2 cycles of 5 consecutive daily doses (0.3 mg/kg/day) (gastric and pancreas). Control animals received an equal volume of vehicle. At the drug doses used in the experiment, no significant toxicity or body weight loss was observed in the treated animals. Tumors in mice treated with Zalypsis® as a single agent strongly reduced their proliferation over the assay period, which finished when paired vehicle-treated animals had to be sacrificed (Fig. 4). Tumor growth reduction ranged from 69% in the Hs746t gastric cancer cell line to 42% in the MiaPaCa-2 pancreas cancer cell line. Tumor growth reductions in the 22RV1 (human prostate cancer), and SW780 (human bladder cancer) xenografts treated with Zalypsis® were 63% and 55%, respectively. The differences in tumor volumes between the vehicle- and the Zalypsis®-treated cohorts were statistically significant ($p < 0.05$) from Day 16 (22RV1, prostate), Day 24 (SW780, bladder), Day 19 (Hs746t, gastric) and Day 22 (MiaPaCa-2, pancreas) until the end of the experiments (Fig. 4).

4. Discussion

In the present work we introduce Zalypsis®, a new synthetic tetrahydroisoquinoline alkaloid that induces DNA damage and apoptosis in a variety of cancer cell lines in the low nanomolar range and shows a potent antitumor activity in several mouse xenograft models.

We first investigated whether Zalypsis® was able to bind either naked or methylated DNA through band shift assays, a methodology that has been previously used for similar analysis with other alkylating agents [13,15,20]. Zalypsis® was able to bind to both a naked PCR product of 250 bp with multiple guanines spread over its whole length and an oligonucleotide with a single binding site. This binding was dependent on the presence of the reactive carbinolamine moiety in the drug since ET-745, a related compound without this reactive group, did not produce any band shifts at any of the concentrations tested. Furthermore, Zalypsis® was able to bind to guanines that are preceded by a methylated cytosine (CpG natural methylation sites), demonstrating that methylation in the major groove does not affect binding of the drug to the minor groove.

Structurally, Zalypsis® belongs to a family of compounds that bind to the exocyclic amino group of guanines in the DNA double helix through an iminium intermediate generated *in situ* by dehydration of the carbinolamine moiety present in the A-ring [4,6–8]. The resulting adduct is additionally stabilized through van der Waals interactions and the establishment of one or more hydrogen bonds with surrounding nucleotides [8,9,21]. In fact, hydrogen bonding rules seem to determine the binding sequence specificity of the tetrahydroisoquinoline family of drugs [9,15]. Considering the diversity of regulatory mechanisms that rely on specific DNA sequences, it can be speculated that sequence selectivity may drive therapeutic specificity for the different DNA-binding compounds. Thus, while guanines are the target of many agents that alkylate DNA, anthramycin selects AGA and AGG triplets [22]; saframycins prefer GGG or GGC [23]; trabectedin favors TGG, CGG, AGC and GGC (while CGA is completely refractory, unlike the *N12*-demethylated analogue ET-729 [15]),

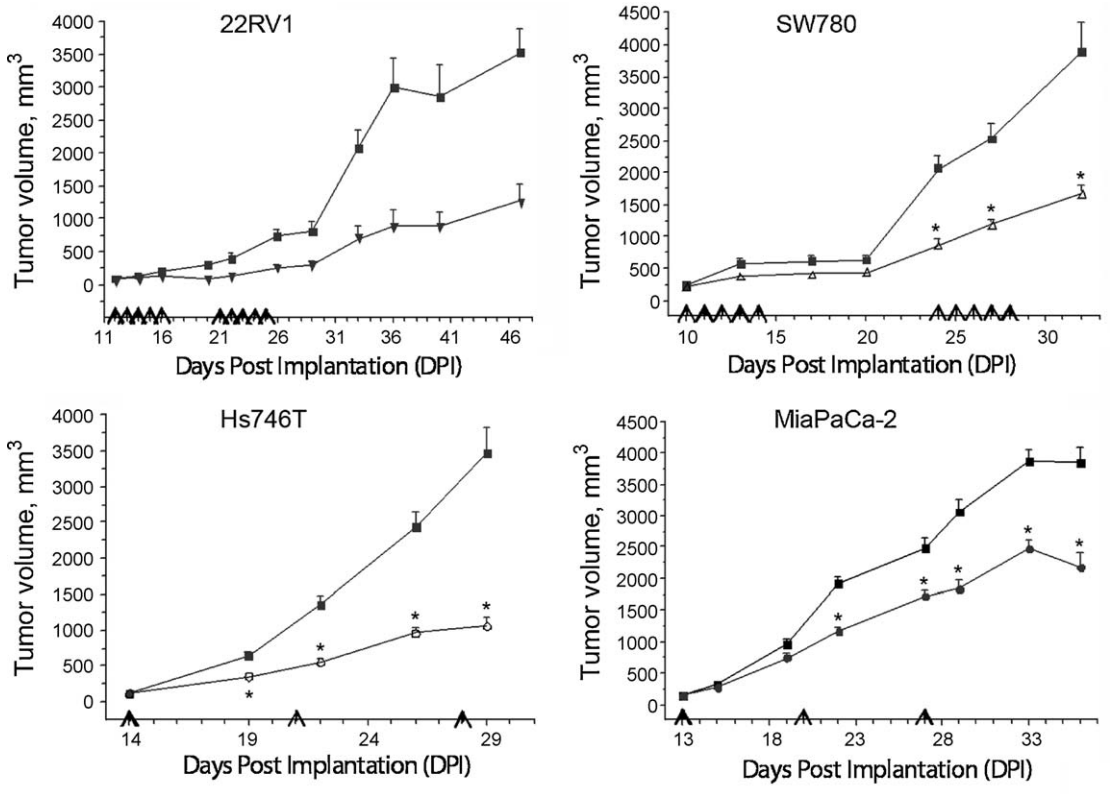

Fig. 4. *In vivo* antitumor activity of Zalypsis®. Treatment with Zalypsis® results in statistically significant ($^{*}p < 0.05$) tumor growth inhibition in 22RV1 prostate (▼), SW780 bladder (△), Hs746t gastric (○), and MiaPaCa-2 pancreas (●) xenograft models compared to vehicle (■) treated animals. Treatments started at a tumor volume size of ca. 150 mm^3 and were intravenously administered either in 2 cycles of 5 consecutive daily doses at 0.3 mg/kg (prostate and bladder) or 3 consecutive weekly doses at 0.9 mg/kg (gastric and pancreas). Each point represents mean ± SEM value ($n = 10$). Arrows indicate dosing days.

and Zalypsis® is shown here to have a preference for GGC, AGC, AGG, TGG and CGG. Whether these subtle differences in sequence selectivity may eventually generate differences in activity against diverse tumor types, is presently not known. On the other hand, the average DNA stabilization brought about on the double helix by drug binding (ΔT_m (max)) was different for Zalypsis® (~10 °C) compared to Yondelis® (~20 °C) (Supplementary Figure 1) [10] although it is still as high as that caused by a tight-binding bisintercalating agent such as echinomycin or thiocoraline [14]. The differences in reactivity and stabilization found for the rather comprehensive collection of alternative DNA triplets containing a central guanine could be rationalized on the basis of molecular models that showed the importance of specific hydrogen-bonding interactions involving drug and DNA atoms in the minor groove for attaining a suitable geometry for nucleophilic attack and covalent adduct formation.

We then verified that Zalypsis® induces DSBs in human cancer cells other than those from multiple myeloma for which γ-H2AX foci formation following exposure to this compound has been recently reported [24]. Indeed, our data show that drug treatment at nanomolar concentrations for 6 h gives rise to a high proportion of positive cells with abundant γ-H2AX foci per cell, as well as comets with a considerable percentage of DNA in the tail. Taken together, these findings most likely indicate that the Zalypsis®–DNA adducts are eventually transformed into DSBs in replicating cells. This is not surprising in light of similar findings recently reported for Yondelis® [10] but there still might be some differences in the way both compounds induce these DSBs. In fact, it has already been demonstrated that in Yondelis®-treated cells, stalling of the transcription-coupled NER (TC-NER) machinery at the adduct position is largely responsible for the toxicity of the compound [25,26]. In this action, the C-ring present in Yondelis®, which protrudes from the DNA minor groove, has been proposed to be directly involved in a hydrogen-bonding interaction with a key basic residue of the NER endonuclease XPG [27]. Since the ring in Zalypsis® that sticks out of the DNA minor groove is very different, this type of interaction may not take place and the repair complex can be stalled at a different step or even proceed further allowing in this case the effective repair of the DNA adducts. Preliminary data support this view as fission yeast mutants defective in the XPG orthologue Rad13 have been shown to be partially resistant to Yondelis® but not to Zalypsis® [28]. We can then envisage the possibility that Zalypsis® behaves as other alkylating/crosslinking agents giving rise to DNA adducts that escape repair by the NER machinery and eventually lead to replication fork stalls in the S-phase, followed by translesion synthesis (TLS) and generation of DSBs (reviewed in [29]). Moreover, the recent finding that Zalypsis® inhibits transcription with a higher potency than Yondelis® [11,12] may indicate that this latter drug principally targets TC-NER-dependent DNA repair whereas Zalypsis® blocks transcription through a stalled initiation or early elongation complex.

In this regard, the data presented here show that Zalypsis® induces an S-phase arrest at both low and high nanomolar concentrations. During S-phase, cells are continuously checking the integrity of their DNA to ensure the accuracy of the copying process. If any alteration is found, there are two safety mechanisms (DNA damage and DNA replication checkpoints) that stop S-phase progression and coordinate the repair of damaged DNA [29–31]. Thus, our data suggest that DNA damage induced by this drug arrests cells in S-phase and activates the DNA replication checkpoints. This scenario is different from that obtained in multiple myeloma cells where Zalypsis® treatment was described to induce an increased in the G_0/G_1 phase [24]. Whether these

effects are cell line- or disease-dependent is presently not known. In our experiments, the S-phase accumulation was higher at 15 nM than at 150 nM. Probably, this is due to a higher cell survival rate at the lower concentration. In fact, although some of the cells treated with high concentrations of Zalypsis® would still accumulate in S-phase, most of them would stop in the cell cycle phase in which they originally were at the onset of drug treatment, due to the high amount of DNA damage that they endure, and they would die with a slower kinetics. Our data also show that Zalypsis®-induced cell death presents the characteristics of apoptosis, with chromatin condensation, dependence on caspase activity and cleavage of the caspase targets PARP-1 and cytokeratin-18. This is in accordance with data obtained in multiple myeloma cell lines on which Zalypsis® treatment induced a strong apoptotic response that was partially dependent on caspase activation [24].

When assayed in a panel of 24 cancer cell lines, Zalypsis® demonstrated a potent cytotoxic activity, with an average IC_{50} of 7 nM in most cell lines, with the notable exception of HCT116 and CAKI-1, both of which are substantially less sensitive to the drug. Myeloma cell lines have also been recently shown to be highly sensitive to Zalypsis®, with IC_{50} values ranging from picomolar to low nanomolar concentrations [24]. Other alkaloids of the tetrahydroisoquinoline family, including jorumycin, renieramycins and saframycins, have been previously shown to possess strong cytotoxic activity, with IC_{50}s also in the low nanomolar range [3,32,33]. According to our data, Zalypsis® exhibits higher cytotoxic activity against leukemia and stomach tumor cell lines, with breast cancer cell lines being less sensitive than the average. This tissue/cell-type sensitivity pattern is clearly different from that observed for Yondelis® as this ecteinascidin shows selectivity against sarcoma, breast, ovary and lung tumor cell lines, with head-and-neck and colon tumor cell lines being slightly less sensitive [34,35].

Finally, the *in vitro* cytotoxicity of Zalypsis® translated well into antitumor activity *in vivo* in four xenograft models of human cancer. The models analyzed corresponded to cell lines ranging from slightly more sensitive (Hs746T, gastric cancer) to substantially less sensitive (SW780, bladder cancer) than the average in the *in vitro* cytotoxicity assays. Zalypsis® demonstrated a clear antitumor activity that was highest for the Hs746t gastric cancer model, with a tumor growth reduction of 69%. The pancreatic cancer model MiaPaCa was the least sensitive to Zalypsis® but, even in this case, the compound achieved a 42% tumor growth reduction. When we assayed the maximum tolerated dose of the drug in two different administration regimes no significant differences among them and no toxic effects to the animals were observed.

In summary, we have demonstrated highly potent *in vitro* and *in vivo* anticancer activities of Zalypsis® and gained some insight into its molecular mechanism of action. This agent exerts its anticancer effects through the covalent modification of guanines in the DNA minor groove that eventually give rise to DNA double-strand breaks, S-phase arrest and apoptosis in cancer cells. These encouraging results strongly support its development as a novel anticancer agent with a view to a wide spectrum of clinical settings.

Appendix A. Supplementary data

Supplementary data associated with this article can be found, in the online version, at doi:10.1016/j.bcp.2009.04.003.

References

[1] Fontana A, Cavaliere P, Wahidullah S, Naik CG, Cimino G. A new antitumor isoquinoline alkaloid from the marine Nudibranch *Jorunna funebris*. Tetrahedron 2000;56:7305–8.

[2] Frinke JM, Faulkner DJ. Antimicrobial metabolites of the sponge *Reniera sp*.. J Am Chem Soc 1982;104:265–9.

[3] Oku N, Matsunaga S, van Soest RW, Fusetani N. Renieramycin J: a highly cytotoxic tetrahydroisoquinoline alkaloid, from a marine sponge *Neopetrosia sp*.. J Nat Prod 2003;66:1136–9.

[4] Kishi K, Yazawa K, Takahashi K, Mikami Y, Arai T. Structure–activity relationships of saframycins. J Antibiot 1984;37:847–52.

[5] Rinehart K, Holt TG, Fregeau NL, Stroh JG, Keifer PA, Sun F, et al. Ecteinascidins 729, 743, 745, 759A, 759B and 770: potent antitumor agents from the Caribean tunicate *Ecteinascidia turbinate*. J Org Chem 1990;55:4512–5.

[6] Guan Y, Sakai R, Rinehart K, Wang AH. Molecular and crystal structures of Ecteinascidins: potent antitumor compounds from the Caribbean tunicate *Ecteinascidia turbinata*. J Biomol Struct Dyn 1993;10:793–818.

[7] Pommier Y, Kohlhagen G, Bailly C, Waring M, Mazumder A, Kohn KW. DNA sequence- and structure-selective alkylation of guanine N2 in the DNA minor groove by ecteinascidin 743, a potent antitumor compound from the Caribbean tunicate *Ecteinascidia turbinata*. Biochemistry 1996;35:13303–9.

[8] Moore BM, Seaman FC, Hurley LH. NMR-based model of an Ecteinascidin 743–DNA adduct. J Am Chem Soc 1997;119:5475–6.

[9] Seaman FC, Hurley LH. Molecular basis for the DNA sequence selectivity of ecteinascidin 736 and 743: evidence for a dominant role of direct readout via hydrogen bonding. J Am Chem Soc 1998;120:13028–41.

[10] Casado JA, Rio P, Marco E, Garcia-Hernandez V, Domingo A, Perez L, et al. Relevance of the Fanconi anemia pathway in the response of human cells to trabectedin. Mol Cancer Ther 2008;7:1309–18.

[11] Magro P, Alvarez E, Kolb E, Mandola M, Scotto KW. Characterization of tumor cell response to the novel anti-tumor agent Zalypsis®. In: 98th AACR annual meeting; 2007. p. 1529.

[12] Feuerhahn S. Mechanistic insights into the effect of oxidative lesions and anticancer drugs on RNA pol II transcription and transcription coupled repair. In: Unité 596 Inserm "Institut de génétique et de biologie moléculaire et cellulaire", Université Louis Pasteur Strasbourg I, Strasbourg; 2008. p. 148.

[13] David-Cordonnier MH, Gajate C, Olmea O, Laine W, de la Iglesia-Vicente J, Perez C, et al. DNA and non-DNA targets in the mechanism of action of the antitumor drug trabectedin. Chem Biol 2005;12:1201–10.

[14] Negri A, Marco E, Garcia-Hernandez V, Domingo A, Llamas-Saiz AL, Porto-Sanda S, et al. Antitumor activity, X-ray crystal structure, and DNA binding properties of thiocoraline A, a natural bisintercalating thiodepsipeptide. J Med Chem 2007;50:3322–33.

[15] Marco E, David-Cordonnier MH, Bailly C, Cuevas C, Gago F. Further insight into the DNA recognition mechanism of trabectedin from the differential affinity of its demethylated analogue ecteinascidin ET729 for the triplet DNA binding site CGA. J Med Chem 2006;49:6925–9.

[16] Redon C, Pilch D, Rogakou E, Sedelnikova O, Newrock K, Bonner W. Histone H2A variants H2AX and H2AZ. Curr Opin Genet Dev 2002;12:162–9.

[17] Guirouilh-Barbat J, Redon C, Pommier Y. Transcription-coupled DNA double-strand breaks are mediated via the nucleotide excision repair and the Mre11-Rad50-Nbs1 complex. Mol Biol Cell 2008;19:3969–81.

[18] Norbury CJ, Zhivotovsky B. DNA damage-induced apoptosis. Oncogene 2004;23:2797–808.

[19] Kramer G, Erdal H, Mertens HJ, Nap M, Mauermann J, Steiner G, et al. Differentiation between cell death modes using measurements of different soluble forms of extracellular cytokeratin 18. Cancer Res 2004;64:1751–6.

[20] David-Cordonnier MH, Laine W, Lansiaux A, Rosu F, Colson P, de Pauw E, et al. Covalent binding of antitumor benzoacronycines to double-stranded DNA induces helix opening and the formation of single-stranded DNA: unique consequences of a novel DNA-bonding mechanism. Mol Cancer Ther 2005;4:71–80.

[21] Garcia-Nieto R, Manzanares I, Cuevas C, Gago F. Bending of DNA upon Binding of ecteinascidin 743 and phthalascidin 650 studied by unrestrained molecular dynamics simulations. J Am Chem Soc 2000;122:7172–82.

[22] Pierce JR, Nazimiec M, Tang MS. Comparison of sequence preference of tomaymycin- and anthramycin–DNA bonding by exonuclease III and lambda exonuclease digestion and UvrABC nuclease incision analysis. Biochemistry 1993;32:7069–78.

[23] Rao KE, Lown JW. DNA sequence selectivities in the covalent bonding of antibiotic saframycins Mx1, Mx3, A, and S deduced from MPE.Fe(II) footprinting and exonuclease III stop assays. Biochemistry 1992;31:12076–82.

[24] Ocio EM, Maiso P, Chen X, Garayoa M, Alvarez-Fernandez S, San-Segundo L, et al. Zalypsis: a novel marine-derived compound with potent antimyeloma activity that reveals high sensitivity of malignant plasma cells to DNA double strand breaks. Blood 2008;113:3781–91.

[25] Erba E, Bergamaschi D, Bassano L, Damia G, Ronzoni S, Faircloth GT, et al. Ecteinascidin-743 (ET-743), a natural marine compound, with a unique mechanism of action. Eur J Cancer 2001;37:97–105.

[26] Takebayashi Y, Pourquier P, Zimonjic DB, Nakayama K, Emmert S, Ueda T, et al. Antiproliferative activity of ecteinascidin 743 is dependent upon transcription-coupled nucleotide-excision repair. Nat Med 2001;7(8):961–6.

[27] Herrero AB, Martin-Castellanos C, Marco E, Gago F, Moreno S. Cross-talk between nucleotide excision and homologous recombination DNA repair pathways in the mechanism of action of antitumor trabectedin. Cancer Res 2006;66:8155–62.

[28] Herrero A, Marco E, García-Hernández V, Martín-Castellanos C, Domingo A, Alvarez E, et al. Resilience of the cytotoxic effects of Zalypsis® (pm00104) to the lack of a functional nucleotide excision repair system. In: American association for cancer research annual meeting; 2007. p. A3470.

[29] Andreassen PR, Ho GP, D'Andrea AD. DNA damage responses and their many interactions with the replication fork. Carcinogenesis 2006;27:883–92.

[30] Zhou BB, Elledge SJ. The DNA damage response: putting checkpoints in perspective. Nature 2000;408:433–9.

[31] Hakem R. DNA-damage repair: the good, the bad, and the ugly. Embo J 2008;27:589–605.
[32] Arai T, Takahashi K, Nakahara S, Kubo A. The structure of a novel antitumor antibiotic, saframycin A. Experientia 1980;36:1025–7.
[33] Lane JW, Estevez A, Mortara K, Callan O, Spencer JR, Williams RM. Antitumor activity of tetrahydroisoquinoline analogues 3-epi-jorumycin and 3-epi-renieramycin G. Bioorg Med Chem Lett 2006;16:3180–3.
[34] Poindessous V, Koeppel F, Raymond E, Comisso M, Waters SJ, Larsen AK. Marked activity of irofulven toward human carcinoma cells: comparison with cisplatin and ecteinascidin. Clin Cancer Res 2003;9:2817–25.
[35] Koeppel F, Poindessous V, Lazar V, Raymond E, Sarasin A, Larsen AK. Irofulven cytotoxicity depends on transcription-coupled nucleotide excision repair and is correlated with XPG expression in solid tumor cells. Clin Cancer Res 2004;10:5604–13.